Hidden zero-temperature bicritical point in the two-dimensional anisotropic Heisenberg model: Monte Carlo simulations and proper finite-size scaling

Chenggang Zhou,[1,2] D. P. Landau,[2] and T. C. Schulthess[1]
[1]*Center for Nanophase Materials Science and Computer Science and Mathematics Division, Oak Ridge National Laboratory, P.O. Box 2008, Oak Ridge, Tennessee 37831-6493, USA*
[2]*Center for Simulational Physics, University of Georgia, Athens, Georgia 30602, USA*
(Received 31 May 2006; published 11 August 2006)

By considering the appropriate finite-size effect, we explain the connection between Monte Carlo simulations of two-dimensional anisotropic Heisenberg antiferromagnet in a field and the early renormalization group calculation for the bicritical point in $2+\epsilon$ dimensions. We found that the long-length-scale physics of the Monte Carlo simulations is indeed captured by the anisotropic nonlinear σ model. Our Monte Carlo data and analysis confirm that the bicritical point in two dimensions is Heisenberg-like and occurs at $T=0$; therefore the uncertainty in the phase diagram of this model is removed.

DOI: 10.1103/PhysRevB.74.064407 PACS number(s): 75.40.Mg, 05.10.Cc, 05.70.Jk, 75.10.−b

I. INTRODUCTION

The two-dimensional anisotropic Heisenberg antiferromagnet has recently been restudied with extensive Monte Carlo simulations.[1] Twenty-five years after the first attempt to delineate its phase diagram with Monte Carlo simulations,[2] many features of it have been clarified. However, the nature of the "spin-flop transition" has been an issue under debate, because the data from the simulations have been inadequate to show unambiguously the thermodynamic limit of the phase boundaries. There is no spin-flop transition in the thermodynamic limit according to renormalization group (RG) calculations in $2+\epsilon$ dimensions.[3–5] Instead, there are two neighboring second-order phase boundaries and a disordered phase in between. By tracing the phase boundaries from high to low temperatures, only an upper bound for the bicritical temperature can be claimed. Below this temperature, an apparent first-order spin-flop transition is indeed observed in both Monte Carlo simulations and neutron scattering experiments on quasi-two-dimensional Heisenberg antiferromagnetic systems with anisotropy.[6] It has been generally agreed that the existing data are consistent with the RG predictions, although some features near the spin-flop line, e.g., the apparent hysteresis[2] and unexpected crossing points in the Binder cumulant,[1] have not been accounted for.

In this paper, we study the spin-flop transition of the *XXZ* model defined by the Hamiltonian

$$\mathcal{H} = J\sum_{\langle i,j\rangle}[\Delta(S_i^x S_j^x + S_i^y S_j^y) + S_i^z S_j^z] - H\sum_i S_i^z. \qquad (1)$$

Here S_i^x, S_i^y, and S_i^z are three components of a unit vector located on site i of a square lattice with periodic boundary conditions in both directions. The anisotropy is given by the parameter Δ, and H is the external magnetic field in the z direction. By the term "spin-flop transition," we refer to the boundary region between the antiferromagnetic (AF) phase and the *XY* phase where two separate second-order phase boundaries cannot be identified in simulations of finite-size systems. We set $J=1$ and $\Delta=4/5$ for simplicity. Our results are expected to be valid for $0<\Delta<1$, since no qualitatively different behavior has been found for other values of Δ, and the phase diagram for $\Delta=4/5$ is most accurately known.[1]

At low temperatures and in a low magnetic field, systems described by Eq. (1) exhibit an Ising-like AF phase, where the order parameter, i.e., the staggered magnetization in the z direction, has a finite value. Above a sufficiently large magnetic field, which is a function of temperature, the AF phase is replaced by an *XY* phase, where the order parameter, i.e., the in-plane staggered magnetization, has a finite value in the finite-size system due to the power-law decay of its correlation function. As pointed out in Ref. 1, there are three different possible scenarios for this spin-flop transition. (a) It is a first-order phase transition at low temperature; the first-order phase boundary and the second-order phase boundaries of the *XY* phase and the AF phase meet at a bicritical point. (b) The bicritical point appears at zero temperature with a very narrow disordered phase separating the *XY* and AF phases. (c) A "biconical phase," in which both order parameters are nonzero, separates the *XY* and the AF phases. These three scenarios are shown in Fig. 1 schematically.

Both RG calculations[7] and the Monte Carlo simulation[8] have shown that (a) is realized in three dimensions, a scenario that is consistent with the finite critical temperature of the three-dimensional isotropic Heisenberg model. In two dimensions, as a result of the Mermin-Wagner theorem,[9] such a bicritical point can only be at zero temperature, and the same prediction comes from RG calculations with the nonlinear σ model.[3–5,10–12] Because of the limited computer power that was then available, early Monte Carlo simulations with the Hamiltonian of Eq. (1) did not favor any of the above three scenarios.[2] Recently, Ref. 1 has found Ising-like scaling behavior in the specific heat and susceptibility on a spin-flop line at $T/J=0.33$ for $\Delta=4/5$, which gives an upper bound in temperature for the bicritical point. We have reproduced these scaling behaviors in our simulations; however, our simulations at lower temperatures do not display such Ising-like scaling behavior, as we will show in this paper. Scenario (c) is realized in systems with random fields[13] or spins with more than four components, e.g., the SO(5) theory.[14] It is unlikely to be the case based on current and previous Monte Carlo simulations.

The main issue to address in this paper is how to compare our extensive data from Monte Carlo simulations of limited

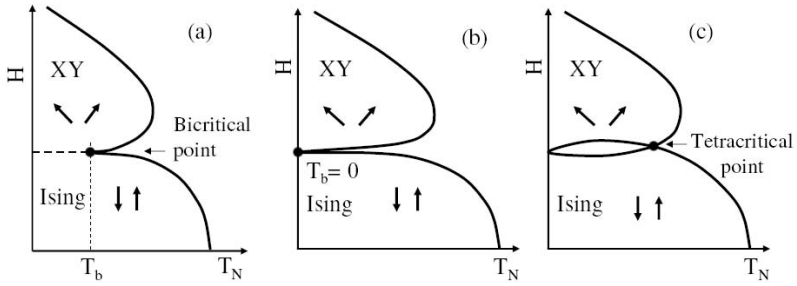

FIG. 1. Three candidates for the phase diagram. Solid lines are second-order phase boundaries, and the dashed line in (a) is a first-order phase boundary.

system sizes with the RG calculations. If they are consistent with each other, we will have a bicritical point at zero temperature in the thermodynamic limit. Otherwise, we are forced to accept the apparent first-order phase transition that we have seen at low temperatures. Because the correlation length is expected to diverge as $\exp(4\pi/T)$ at low temperatures, our computer power is very unlikely to be ample for simulations with system sizes larger than the correlation length in the foreseeable future. Therefore, properly extracting the thermodynamic limit from our data is essential. We will discuss the Monte Carlo simulation and derive the theoretical finite-size scaling predictions in Sec. II, present results from our simulation and the data analysis in Sec. III, and conclusions with discussion in Sec. IV.

II. THEORETICAL BACKGROUND

A. Monte Carlo simulation and traditional finite-size scaling

At zero temperature, the system has a spin-flop transition at $H_c=4J\sqrt{1-\Delta^2}$. The system is in the fully aligned AF configuration for $H<H_c$ and is in the spin-flop configuration for $H>H_c$. As $H\to H_c^+$, the spin-flop configuration approaches $S_i^z=\sqrt{(1-\Delta)/(1+\Delta)}$ and $S_i^{x,y}=(-1)^i n^{x,y}\sqrt{2\Delta/(1+\Delta)}$, where (n^x,n^y) is an arbitrary unit vector. Obviously, the spin-flop transition is a first-order phase transition at zero temperature, since the order parameter (staggered magnetization) exhibits a discontinuity. In scenario (a) in Fig. 1, the spin-flop line starts from H_c at $T=0$, shows a small positive slope as the temperature increases, and eventually develops into an umbilicus, where the AF-paramagnetic phase boundary and the XY-paramagnetic phase boundary are clearly separated. For the other possibilities in two dimensions, two phase boundaries might well be indistinguishable from each other but yield the same "effective" finite-temperature behavior.

We perform Monte Carlo simulations that scan the magnetic field across the spin-flop transition at constant temperatures. The random spin configurations are generated with the heatbath algorithm,[15] which has been recently shown to be the optimal single-spin algorithm for Heisenberg spins.[16,17] It is a rejection-free algorithm due to the fact that the probability distribution $P(\mathbf{S})\propto\exp(\mathbf{h}\cdot\mathbf{S}/T)$ of a single spin subject to a magnetic field can be produced with uniform random number generators without rejecting trial flips. As in Ref. 17, we simultaneously perform two simulations with different initial configurations, the equilibrium is achieved by letting these two simulations run until their order parameters are almost equal. Each simulation then runs for 10^6–10^7 Monte Carlo steps per spin at the given temperature and magnetic field, and is allowed to accumulate substantially more data near the critical magnetic field. The data for energy, magnetization, and staggered magnetization are stored for histogram reweighting. The difference in observables measured from independent simulations is used to estimate the error bar. Totally we have spent about 1 CPU yr and accumulated 27 gigabytes of data, which represents a modest computing load on a decent Linux cluster.

We calculate the ensemble average of the staggered magnetization:

$$\mathbf{M}^\dagger = \frac{1}{L^2}\sum_i (-1)^i \mathbf{S}_i, \tag{2}$$

where the sign is different on the two sublattices. We define the tilt angle θ between the z axis and $\mathbf{M}^\dagger$ as

$$\theta = \cos^{-1}\frac{|M_z^\dagger|}{|M^\dagger|}, \tag{3}$$

where the value of θ is restricted to $[0,\pi/2]$ due to the inversion symmetry of the staggered magnetization, and calculate its probability distribution. The Binder cumulant for an arbitrary observable X is defined as

$$U_4(X) = 1 - \frac{\langle X^4\rangle}{3\langle X^2\rangle^2}, \tag{4}$$

where $\langle\cdots\rangle$ denotes the ensemble average. The susceptibility per spin of $M_z^\dagger$ is defined as

$$\chi = \frac{L^2}{T}[\langle (M_z^\dagger)^2\rangle - \langle |M_z^\dagger|\rangle^2], \tag{5}$$

and the specific heat per spin is defined as

$$c_v = \frac{L^2}{T^2}(\langle E^2\rangle - \langle E\rangle^2), \tag{6}$$

where E is the internal energy per site.

In order to determine the type of phase transition, we performed the traditional finite-size scaling analysis. In the case of an Ising-like second-order phase transition, the specific heat exponent $\alpha=0$, because c_v is logarithmically divergent near the critical temperature or critical field, and its maximum value increases as $\ln L$. The localization length exponent $\nu=1$; the spontaneous magnetization exponent $\beta=1/8$; and the susceptibility exponent $\gamma=7/4$. In case of a first-order phase transition, these exponents can also be defined properly, and they have a different set of values:[18] α

$=1$, $\beta=0$, $\nu=1/2$, $\gamma=1$. (In general $\nu=1/d$, where d is the dimensionality of the system.) Near the phase transition point, it is convenient to define the reduced temperature $t=T/T_c-1$ and reduced field $h=H/H_c-1$. Finite-size scaling theory predicts the following scaling relations:

$$\langle (M_z^\dagger)^2 \rangle_L = L^{-2\beta/\nu} \mathcal{M}(tL^{1/\nu}), \tag{7}$$

$$\langle \chi \rangle_L = L^{\gamma/\nu} \mathcal{C}(tL^{1/\nu}). \tag{8}$$

Similar relations hold for $(M_x^\dagger)^2+(M_y^\dagger)^2$ and c_v, as well as for transitions with h as the control variable. In particular, for c_v of Ising-like transition, the prefactor $L^{\alpha/\nu}$ is replaced by $C+\ln L$, where C is a constant.

B. Low-temperature finite-size scaling predictions

As we shall see from the results in the next section, neither the scaling relations for the first-order phase transition nor those for second-order phase transitions fit our data perfectly well. The first-order phase transition apparently seems to be more consistent though. To resolve these discrepancies, we return to the RG calculation of bicritical phenomenon in $2+\epsilon$ dimensions. The long-length-scale physics is expected to be governed by the nonlinear σ model with an anisotropy term:[3,4]

$$\mathcal{H}_\sigma = -\frac{1}{2T}\int d^dx[(\partial_\mu \pi)^2 + (\partial_\mu \sigma)^2 + g\sigma^2], \tag{9}$$

where the $O(3)$ spin field $(\pi_1(x), \pi_2(x), \sigma)$ satisfies the constraint $\pi^2+\sigma^2=1$ and the anisotropy constant $g \propto H-H_c$. [Note: we follow the convention in Ref. 4 here, so the Boltzmann factor is $\exp(\mathcal{H}_\sigma)$.] In general, g is expected to be a linear combination of both magnetic field and temperature contributions:[19] $g=a(H^2-H_c^2)+b(T-T_c)$. The spin-flop line (defined by $g=0$) of our model is almost horizontal, with a very small negative b. In the scenario shown in Fig. 1(b), H_c actually falls in the paramagnetic phase between two phase boundaries. The RG calculation can proceed with either the momentum shell renormalization technique[4] or Polyakov's approach.[3,10] The same results can also be derived with Brézin and Zinn-Justin's method.[11,12] The RG flow differential equations for renormalized temperature $T(l)$ and anisotropy constant $g(l)$ are

$$\frac{dT(l)}{dl} = -\epsilon T(l) + \frac{T(l)^2}{2\pi}\left(n-3+\frac{1}{1+g(l)}\right), \tag{10}$$

$$\frac{dg(l)}{dl} = 2g(l) - \frac{T(l)}{\pi}\frac{g(l)}{1+g(l)}, \tag{11}$$

where $\epsilon=d-2$. For our present purpose, it is sufficient to set $\epsilon=0, n=3$, and keep the lowest-order terms of g in these equations. The approximate solution then reads

$$T(l) = \frac{2\pi T}{2\pi - Tl}, \tag{12}$$

$$g(l) = ge^{2l}T^2/T(l)^2 = ge^{2l}[1-Tl/(2\pi)]^2. \tag{13}$$

Additionally, the equation for the renormalization constants for π and σ can be derived from Ref. 4:

$$\frac{d\ln\zeta_\pi}{dl} = d - \frac{T(l)}{4\pi}\frac{g(l)+2}{g(l)+1}, \tag{14}$$

$$\frac{d\ln\zeta_\sigma}{dl} = d - \frac{T(l)}{2\pi}. \tag{15}$$

Using Eq. (12) and $d=2$, for negligible g, one finds that ζ_π and ζ_σ are both given by

$$\zeta_\sigma = \zeta_\pi = e^{2l}\left(1-\frac{Tl}{2\pi}\right). \tag{16}$$

These results imply that for $g>0$, the renormalization flow goes to $g=+\infty$, which corresponds to the XY model; for $g<0$, it goes to $g=-\infty$, which corresponds to the two-dimensional Ising model; for $g=0$, it goes to the high-temperature paramagnetic phase, which is consistent with the Mermin-Wagner theorem.[9] Conventionally, the thermodynamic quantities are calculated by integrating the renormalization flow equation to a characteristic scale l^*, for which $g(l^*)=O(1)$. The corresponding thermodynamic quantities can be calculated by other means, e.g., perturbation theory. Then a trajectory integral "matching" formalism[4,20–22] is used to obtain these quantities at the original scale $l=0$. For example, the susceptibility has the scaling form $\chi(T,g) \sim e^{4\pi/T}\Phi(ge^{4\pi/T})$ for small T and g in the thermodynamic limit,[4] which is analogous to the crossover phenomenon of a finite-temperature bicritical point.[23,24] The Ising or XY critical behavior is contained in the scaling function Φ, which is calculated from the effective Ising or XY model (depending on the sign of g) at the scale $l^* \sim e^{4\pi/T}$. Due to the finite size of the systems in our simulations, the above RG flow cannot go very far in the RG flow diagram for an infinite system, but only to the scale set by the system size $l' \approx \ln(L/a)$, where a is the microscopic lattice constant (fixed to be unity). For our model, $L=100a$ is not a large system size compared to the correlation length, so we expect that the lowest-order solutions Eqs. (12) and (13) are sufficient. In the real-space RG terminology,[25] at scale l', the spins in a block of linear size $e^{l'}$ are effectively replaced by a single block spin; therefore, we expect that our simulation with system size L in a magnetic field sufficiently close to the critical field is governed by the simple Hamiltonian

$$\mathcal{H}_{\text{eff}} = -q\sigma^2, \tag{17}$$

where the coefficient q is given by

$$q = \frac{g(\ln L)}{2T(\ln L)} = \frac{gL^2}{2T}\left(1-\frac{T\ln L}{2\pi}\right)^3. \tag{18}$$

Near the spin-flop transition, $g=k(T,L)h+O(h^2)$, where h is the reduced field, and we expect the coefficient $k(T,L)$ to weakly depend on T and L. As a result, the free energy should appear as a function of $hT^{-1}L^2[1-T\ln L/(2\pi)]^3$. One can define a "correlation length exponent" $\nu=1/2$, based on

the leading L^2 dependence. The staggered magnetization also has to contain a factor from the spin renormalization constant:

$$\langle (M_z^\dagger)^2 \rangle_L = L^{-4} \zeta_\sigma^2 \langle \sigma^2 \rangle_{\mathcal{H}_{\text{eff}}}, \tag{19}$$

$$\langle (M_{xy}^\dagger)^2 \rangle_L = \langle (M_x^\dagger)^2 + (M_y^\dagger)^2 \rangle_L = L^{-4} \zeta_\pi^2 \langle \pi^2 \rangle_{\mathcal{H}_{\text{eff}}}, \tag{20}$$

where $\langle \cdots \rangle_{\mathcal{H}_{\text{eff}}}$ denotes the thermal average with respect to the effective Hamiltonian Eq. (17). When $\zeta_\sigma / \zeta_\pi \approx 1$, both of them have the scaling form:

$$\left(1 - \frac{T \ln L}{2\pi}\right)^2 \mathcal{F}_{\parallel,\perp}\left[\frac{hL^2}{T}\left(1 - \frac{T \ln L}{2\pi}\right)^3\right]. \tag{21}$$

Furthermore, the distribution of $\mathbf{M}^\dagger$ should be on a sphere of radius $1 - T \ln L/(2\pi)$; the distribution of its tilt angle has the form

$$P(\theta) = Y^{-1} \exp(-q \cos^2 \theta) \sin \theta, \tag{22}$$

where Y is a normalization constant. At the critical field $g=h=0$, the above distribution is uniform. Consequently the critical Binder cumulant for $\cos \theta$ is $U_4(\cos \theta) = 2/5$. $U_4(M_z^\dagger)$ should also be close to this value, with a small negative correction due to the longitudinal fluctuation of $\mathbf{M}^\dagger$. The maximum susceptibility corresponds to the maximum fluctuation in σ, so the following scaling formula is expected:

$$\chi = \frac{\zeta_\sigma^2}{L^2} \mathcal{X}\left[\frac{hL^2}{T}\left(1 - \frac{T \ln L}{2\pi}\right)^3\right]. \tag{23}$$

One can again define a susceptibility exponent $\gamma = 1$ based on the leading L^2 dependence, which is assumed to be $L^{\gamma/\nu}$. The critical exponent ratio is then identical to that for a first-order phase transition; therefore, the logarithmic corrections are required to determine whether the spin-flop transition is a first-order phase transition or not.

To calculate the specific heat, the standard approach is to derive it from the free energy $f = -L^{-2} \ln Z$. As in Ref. 4, we perform a trajectory integral from $l=0$ to l^* to evaluate the free energy. For clarity of our discussion, we reproduce the trajectory integral formula from Ref. 4 here:

$$f(T,g) = \int_0^{l^*} e^{-dl} G_0(l) dl + e^{-dl^*} f[T(l^*), g(l^*)], \tag{24}$$

in which we set $d=2$ in our calculation and the kernel G_0 depends on both the on-shell Green's function and the spin renormalization factors. With the final scale $l^* = \ln L$ and the approximate solution Eqs. (12) and (13), this trajectory integral can be evaluated analytically with the technique in Appendix A of Ref. 22. Among many terms in the result, we are particularly interested in those of the form $L^{-2} f_s[T(l^*), g(l^*)]$, for reasons which will soon become clear. It turns out that the only such term is $f_s[g(l^*)] = -\ln[1 + g(l^*)]$. The last term in Eq. (24) is given by the single-spin Hamiltonian Eq. (17):

$$L^{-2} F\left[\frac{gL^2}{2T}\left(1 - \frac{T \ln L}{2\pi}\right)^3\right], \tag{25}$$

where

$$F(q) = -\ln \int_0^\pi \exp(-q \cos^2 \theta) 2\pi \sin \theta \, d\theta. \tag{26}$$

The divergent term in the specific heat is given by

$$c_v = -\frac{\partial}{\partial T}\left(T^2 L^{-2} \frac{\partial (F + f_s)}{\partial T}\right). \tag{27}$$

One would expect the leading divergent term in Eq. (27) is proportional to $L^2 g^2$, with multiplicative logarithmic corrections. However, obviously on the spin-flop line $g=0$, this term vanishes. This dilemma is solved by noting that T in Eq. (27) is the real temperature at which the simulation is performed, while T in Eqs. (24) and (25) is a renormalized temperature for the long-length-scale effective Hamiltonian, and from now on it will be denoted T^*. The spin-flop line does not follow a constant temperature; in other words, the effective anisotropy g is also a function of T. If we change T in the simulation, we actually change the effective anisotropy g, which could drive the system to cross the spin-flop line. Therefore, the partial derivative in Eq. (27) should be written as

$$\frac{\partial}{\partial T} = a \frac{\partial}{\partial T^*} + b \frac{\partial}{\partial g}. \tag{28}$$

Two derivatives $\partial / \partial g$ acting on $L^{-2} F$ would produce a divergent term proportional to $L^2 [1 - T^* \ln L/(2\pi)]^6$. Similarly, f_s results in a divergent term proportional to $L^2 [1 - T^* \ln L/(2\pi)]^4$. After all these considerations, the divergent part of the specific heat is expected to have the following scaling form:

$$c_v = L^2 x^6 \mathcal{C}_6(hL^2 x^3) + L^2 x^4 \mathcal{C}_4(hL^2 x^3), \tag{29}$$

where $x = 1 - T^* \ln L/(2\pi)$. If the spin-flop line is perfectly horizontal, i.e., $b=0$, there will not be a peak in the specific heat. We expect the $\mathcal{C}_6$ term to be dominant in Eq. (29), because F also contributes a factor T^{-2} after being differentiated twice; on the other hand, a straightforward calculation shows that the $\mathcal{C}_4$ term does not show a peak at $g=0$, but an asymmetric background.

The above trajectory integral actually connects the intermediate renormalized Hamiltonian Eq. (9) to the final renormalized Hamiltonian Eq. (17). In doing so, we have ignored a similar trajectory integral which connects the bare Hamiltonian Eq. (1) to the intermediate Hamiltonian Eq. (9). Although we cannot write down an analytic expression for its integrand and its final contribution to the free energy, we expect it to depend on the lattice constant, which is the smallest length scale in the system, and an intermediate length scale at which Eq. (9) is valid, but not on the largest length scale L. Therefore, it cannot possibly give rise to an L^2 divergence. For the divergent terms in c_v, it is hence justified to ignore this precursory trajectory integral.

Unlike the conventional finite-size scaling, the above finite-size scaling relations are not expected to hold for very large system sizes, because for sufficiently large L, the phase boundaries of the AF and XY phases become discernible. This obviously happens when $T \ln L \sim 2\pi$, i.e., the spin renormalization constants become very small, corresponding

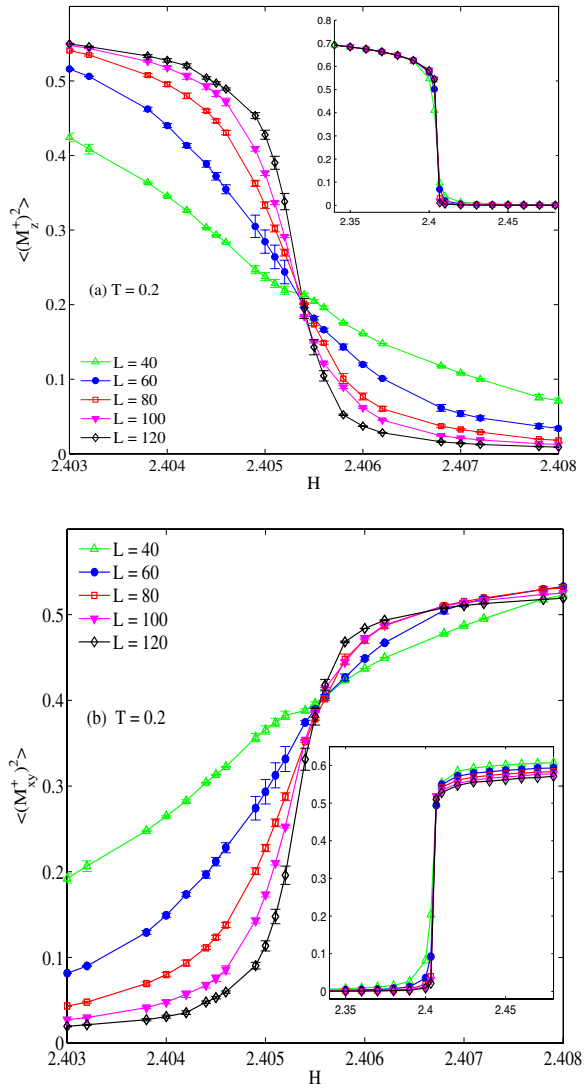

FIG. 2. (Color online) Staggered magnetization across the finite-lattice spin-flop line at $T=0.2$. Each group of nearby data points is from one simulation performed with a single fixed magnetic field. Histogram reweighting was used to calculate observables in slightly different magnetic fields. The insets show the data measured from a larger range of magnetic field.

to a disordered phase. For either large l or large g, the higher-order terms in Eqs. (10) and (11) become non-negligible; therefore, the approximate solution Eqs. (12) and (13) and the above finite-size scaling relations are no longer sufficient. Thus, we expect the above finite-size scaling analysis to be valid for small effective anisotropy, i.e., $H \approx H_c$, and system sizes smaller than the correlation length.

III. DATA AND ANALYSIS

A. Raw data and the apparent first-order phase transition

We first present some representative raw data for the staggered magnetization from simulations with different system sizes, and we will then show traditional finite-size scaling plots. Figure 2 shows the staggered magnetization at $T=0.2$

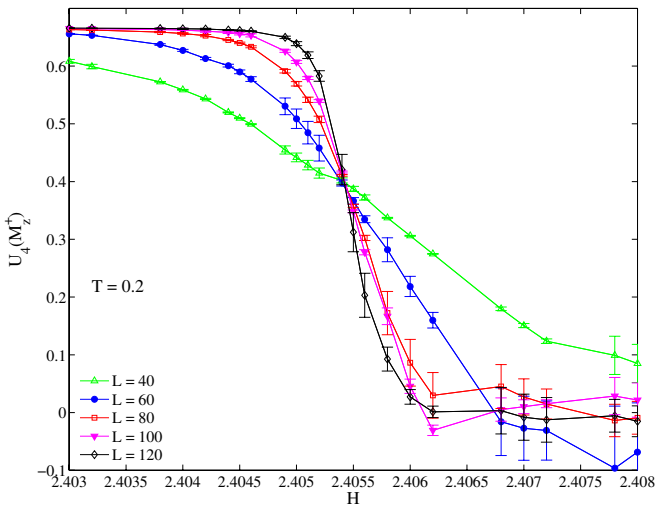

FIG. 3. (Color online) Binder cumulant for various sizes at $T=0.2$. The crossing points of these curves are near $H=2.4055$. U_4 at the crossing point is different from the universal value for an Ising-like transition.

for magnetic fields on both sides of the finite lattice spin-flop transition. The spin-flop transition can be clearly observed, and when viewed at moderate resolution (see the insets) the data suggest a first-order transition. Both $\langle (M_z^\dagger)^2 \rangle$ and $\langle (M_{xy}^\dagger)^2 \rangle$ reach either zero or a large value quickly as H deviates from H_c, which is why we have to zoom in on a very narrow range (0.005 in width) of the magnetic field to see the finite-size effect for relatively large systems. The critical magnetic field that separates the XY phase from the AF phase can already be estimated rather accurately from the size dependence seen in Fig. 2. There is no noticeable sign of an intermediate phase which has zero expectation values for both order parameters. There is also no sign of a region with nonzero values for both order parameters. In the XY phase, we see from the inset of Fig. 2(b) that the saturated values of the order parameter are smaller for larger systems, which is consistent with the property of the XY phase. (We expect the saturated value to decrease as $L^{-2\eta}$, where η is a temperature-dependent exponent.[26,27]) On the other side, in the AF phase, the inset of Fig. 2(a) shows that $\langle (M_z^\dagger)^2 \rangle$ calculated with different system sizes quickly converges to the nonzero thermodynamic limit.

If the spin-flop transition contains an Ising-like transition, then we would expect to see the universal value of the Binder cumulant $U_4^* \approx 0.618$ at the critical magnetic field, therefore we plot $U_4(M_z^\dagger)$ in Fig. 3 to see if it indicates an Ising-like second order phase transition. However, the curves in Fig. 3 cross each other at values close to 0.4, clearly below the Ising universal value. There is not any systematic trend indicating that the crossing point moves up with increasing system size. This result is in agreement with Ref. 1, where it is shown that only when $T>0.4$ do the crossing points in the Binder cumulant curves start to move toward the Ising universal value. As Ref. 1 has shown in the phase diagram, the AF-paramagnetic boundary and XY-paramagnetic boundary are clearly separated for $T>0.4$. We have also calculated the Binder cumulant for $T=0.1$, 0.265, and 0.33, and seen results

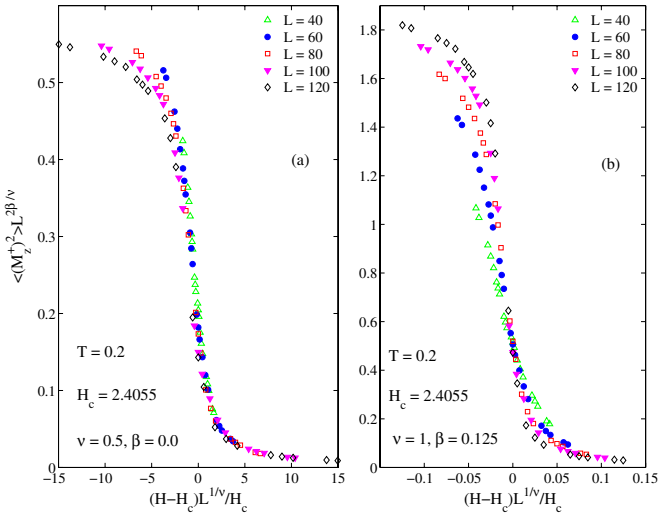

FIG. 4. (Color online) Finite-size scaling of $M_z^\dagger$. (a) Exponents used belong to first-order phase transition; (b) Ising exponents are used. Error bars are not plotted since most of them are smaller than or equal to the size of the symbols, as shown in Fig. 2.

similar to Fig. 3. So it is indeed tempting to consider the possibility of a bicritical point that exists between $T=0.33$ and 0.4.

To see whether our data really fit the behavior expected for a first-order phase transition, we show the finite-size scaling analysis of $M_z^\dagger$ in Fig. 4. According to Eq. (7), all the data points should collapse onto a single curve if we choose the right exponents ν and β. The field dependence of the data in both Fig. 2 and Fig. 3 indicate that H_c is between 2.405 and 2.406. In Fig. 4, we have fine-tuned H_c to collapse the data as much as possible onto a single curve, and found that it is impossible to do so with Ising exponents. With first-order exponents, the scaling plot Fig. 4(a) is clearly better. However, systematic deviations are discernible in the low-field AF phase. In fact, if we allow β to have a small value, we have found that the scaling plot looks best with $\beta=0.031$. The same phenomenon has also been observed in traditional finite-size scaling plots for $\langle(M_{xy}^\dagger)^2\rangle$.

Similar scaling analyses have been done for $T=0.1$ and 0.265. In all those cases, the Ising exponents fail, but the first-order exponents work reasonably well, especially for $T=0.1$. If we accept a small β which goes to zero as T goes to zero, then at finite temperatures, the spontaneous staggered magnetization does decay as $M_z^\dagger \propto |h|^\beta$ in the thermodynamic limit ($L\to\infty$). We would indeed have a second-order phase transition. However, the correlation length exponent $\nu=1/2$ is not consistent with this scenario. For susceptibility and specific heat, finite-size scaling analysis has also ruled out an Ising-like transition as a possible scenario. Especially for the specific heat, its maximum value scales roughly as L^2 at $T=0.1$, 0.2, which is glaringly different from the Ising-like logarithmic behavior.

B. Proper finite-size effect and scaling

To characterize the spin-flop transition, we first study the probability distribution of the staggered magnetization to get

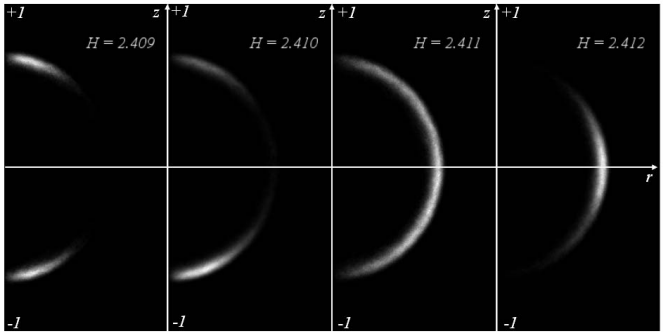

FIG. 5. Probability distribution of the staggered magnetization across the spin-flop transition. $P(r,z)$ is proportional to the gray scale. The data are from simulations with $L=100$ at $T=0.265$.

a vivid picture of the spin-flop transition. Due to the obvious rotational symmetry around the z axis, we plot in Fig. 5 the probability distribution $P(r,z)$ of systems with $L=100$ in cylindrical coordinates at $T=0.265$. It can be clearly seen from this figure that $\mathbf{M}^\dagger$ is distributed on a sphere of about 0.65 in radius. In the AF phase, the distribution is confined to the north and south poles; in the XY phase, the distribution is near the equator. One would naturally define a *finite-size* critical field H_c at which the distribution is uniform on this sphere, i.e., zero effective anisotropy. For $L=100$ and $T=0.265$, we have found $H_c \approx 2.411$ which is in agreement with the observation of $\langle(M_z^\dagger)^2\rangle$ and $U_4(M_z^\dagger)$. At this critical field, $U_4(M_z^\dagger)\approx 2/5$, which can be immediately calculated given this uniform distribution. The same pattern of transition have been observed at different temperatures with different system sizes. For larger systems and higher temperatures, we have observed smaller spheres. Clearly, a finite-size effect can be extracted from these spherical distributions.

To be more quantitative, we calculate the angular distribution of the staggered magnetization. Figure 6 shows the distribution of the tilt angle θ calculated from simulations at

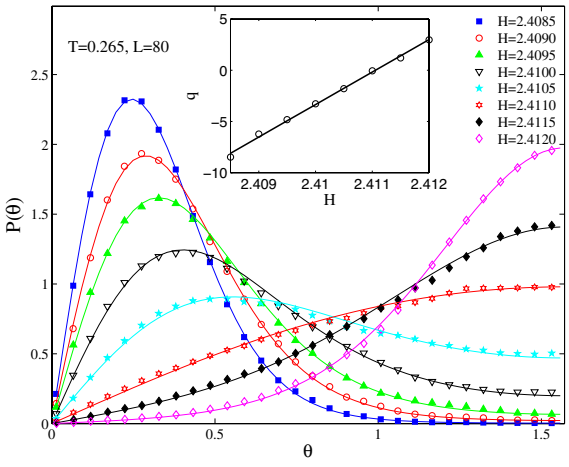

FIG. 6. (Color online) Probability distribution of the tilt angle θ. Symbols are calculated from the histogram of θ in the simulations, and the solid lines are curve fitting with Eq. (22). The fitting parameter q is plotted in the inset, where the straight line is a linear fit. The simulations were performed with $L=80$ at $T=0.265$.

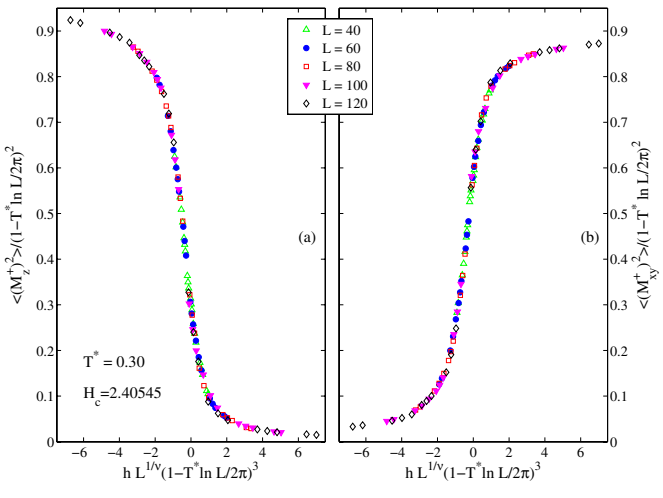

FIG. 7. (Color online) Finite-size scaling analysis corresponding to Eq. (21) at $T=0.2$. (a) The AF order parameter; (b) the XY order parameter. We introduce T^* as a fitting parameter which is slightly above the actual temperature at which the simulation is done. Error bars are smaller than or equal to the size of the symbols.

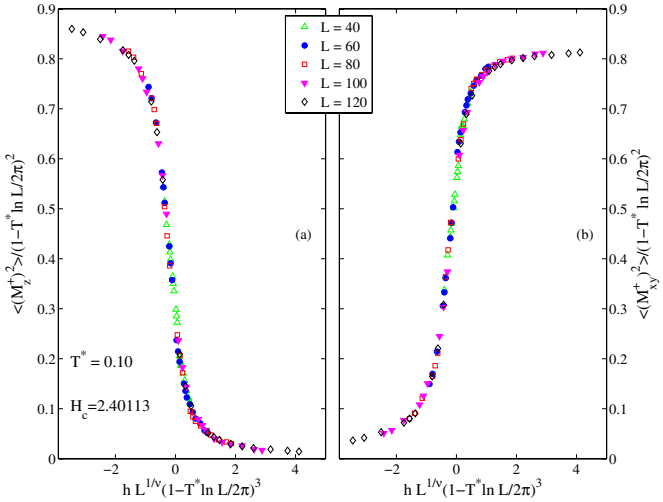

FIG. 8. (Color online) The same as Fig. 7, but for simulations at $T=0.1$. Unlike Fig. 7, we have used $T^*=T$ here.

$T=0.265$ for $L=80$. The data are fitted with Eq. (22), which only has one fitting parameter q. Obviously this simple functional form fits the simulations very well. The inset in Fig. 6 shows the fitting parameter, i.e., Eq. (18), is a linear function of H, which is consistent with our assumption that $g \propto h$. Thus, we have shown that close to H_c, the thermodynamics of the staggered magnetization is indeed governed by the simple Hamiltonian Eq. (17).

The staggered magnetization clearly has a finite value at H_c in the simulations. If this is also true for the thermodynamic limit, then we will have to choose between the scenario of a first-order phase transition, or that of an intermediate ordered phase with a tetracritical point. However, this is not the case for two-dimensional systems. Suppose we enlarge the simulation to a size nL, since we have shown that an $L\times L$ block indeed behaves as an effective Heisenberg spin in an anisotropic potential, the long-length-scale physics should be captured by a Hamiltonian of these block spins. Although microscopically, the anisotropy may have different forms, at a large enough length scale the $g\sigma^2$ term turns out to be the only dominant term, as shown by the probability distribution in Fig. 6. In terms of RG terminology, it is the only relevant perturbation that keeps the z axis rotational symmetry. Since a similar anisotropy in the kinetic energy, $g_1(\partial_\mu \sigma)^2$, has been found to be irrelevant,[3] our simulations have indeed justified Eq. (9) as an appropriate Hamiltonian to analyze the spin-flop transition. Following the RG analysis outlined in Sec. II one would conclude that the behavior in the thermodynamic limit is two second-order phase boundaries and a bicritical point at zero temperature, i.e., that which is shown in Fig. 1(b).

Now we perform a finite-size scaling analysis in order to examine whether or not the logarithmic corrections in Eq. (21) can be seen in the data from the simulations. The renormalized temperature T in the effective Hamiltonian Eq. (9) is, in general, different from the temperature at which the simulation is performed. Therefore, we are allowed to use an extra fitting parameter T^* in Fig. 7 to make the data points collapse better on a single curve. We find that all the data points do collapse onto a single curve in both Figs. 7(a) and 7(b) with the choice $T^*=0.3$. Actually, if this renormalized temperature is not introduced, Fig. 7 still looks clearly better than Fig. 4(a), where we assume a first-order phase transition. In the transition region, we also expect $\langle (M_z^\dagger)^2 + (M_{xy}^\dagger)^2 \rangle$ to be nearly a constant as seen in Fig. 5. This is also consistent with Fig. 7 where the decrease in $\langle (M_z^\dagger)^2 \rangle$ is compensated by the increase in $\langle (M_{xy}^\dagger)^2 \rangle$. A small β improves Fig. 4(a) because a logarithmic correction enters by the Taylor expansion for small β: $L^{2\beta/\nu} \approx 1+2\beta\nu^{-1} \ln L$. Error bars are not plotted in Fig. 7 and the other scaling plots, because most of them are smaller than or equal to the size of the symbols used in these figures. They can be found in Figs. 2 and 3. Figure 8 shows the same scaling analysis for simulations performed at $T=0.1$. We have found that this scaling plot is very clear even without introducing a renormalized temperature. The critical field H_c is fixed up to six significant digits in Figs. 7 and 8 by closely examining the central critical region of very small h. However, one should not push this too far because the apparent existence of a single critical field is only a finite-size effect. For large systems, there are two separate critical fields for the AF phase boundary and the XY phase boundary, respectively. The same finite-size scaling analysis at $T=0.265$ still produces a very good single curve; however, the best scaling is achieved by allowing H_c for the XY phase to be slightly above that for the AF phase, behavior which could be understood as a sign of separating phase boundaries.

The logarithmic correction for $\mathbf{M}^\dagger$ comes from the spin renormalization constants in Eqs. (19) and (20). The effective spin σ and π can be calculated directly from $\mathbf{M}^\dagger$, given that $\zeta_\pi \approx \zeta_\sigma$. One would expect that the finite-size scaling of $\langle \sigma^2 \rangle$ only involves a scaling of the magnetic field. In fact, Eqs. (17) and (18) imply that $\langle \sigma^2 \rangle_L$ for different sizes as well as different temperatures can collapse on to a single curve, provided that $k(T,L)=h/g$ depends weakly on T and L. Figure 9 plots $\langle \sigma^2 \rangle_L$ versus $hT^{-1}L^2(1-T\ln L/2\pi)^3$, and shows

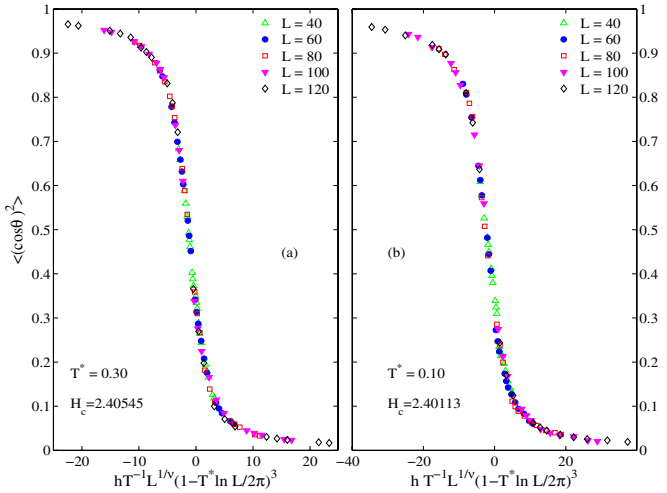

FIG. 9. (Color online) Finite-size scaling plot of the effective σ spin component from simulations at $T=$(a) 0.2 and (b) 0.1. Instead of adjusting T^*, we have simply set $T^*=T$. (a) and (b) are expected to display the same curve; see text for details. Error bars are smaller than or equal to the size of the symbols.

that this is indeed true in the simulations. We have also calculated the Binder cumulant $U_4(\cos\theta)$. Since the longitudinal fluctuation in $\mathbf{M}^\dagger$ is completely projected out, $U_4(\cos\theta)$ is exactly 2/5 at the crossing point, which corresponds to the critical magnetic field for finite-size systems.

As for the susceptibility, we test Eq. (23) by plotting $\chi L^{-2}(1-T\ln L/2\pi)^{-2}$ versus $hL^2(1-T\ln L/2\pi)^3$ in Fig. 10. For $L=40$, 60, and 80, our data collapse onto single curves at $T=0.1$ and 0.2 very well. For two larger sizes $L=100$ and 120, although we have fewer data points near the peak of the susceptibility and a few data points have larger statistical errors than others, they appear to fall on the same curve reasonably well. We have also plotted the data assuming finite-size scaling for an Ising-like transition or a first-order phase transition but found none of those works better than Fig. 10.

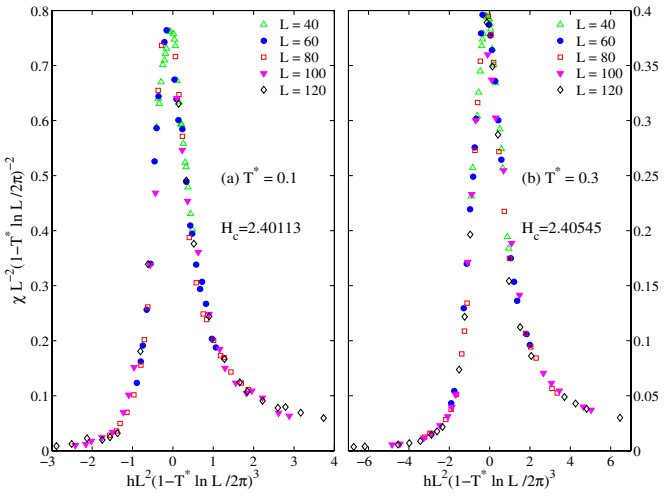

FIG. 10. (Color online) Scaling plot for susceptibility near the spin-flop transition according to Eq. (23), at $T=$(a) 0.1 and (b) at 0.2.

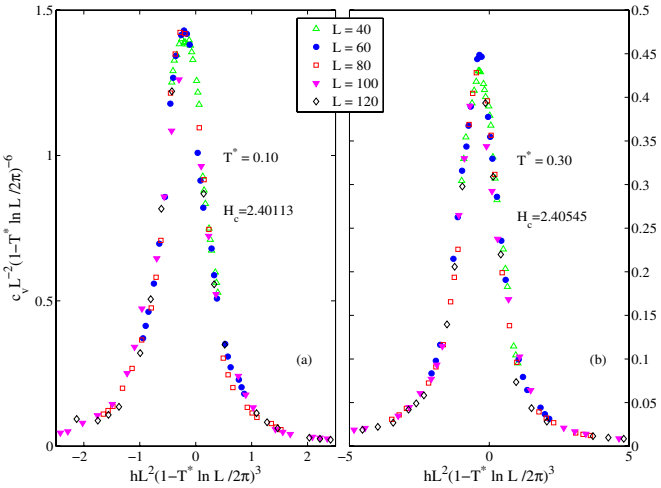

FIG. 11. (Color online) Scaling plot for specific heat near the spin-flop transition according to Eq. (29), at $T=$(a) 0.1 and (b) 0.2.

Finally, in Fig. 11 we show the finite-size scaling plots for specific heat which follow Eq. (29). Only the first $\mathcal{C}_6$ term has been considered here. Most of the data points collapse quite well onto a single curve in both Figs. 11(a) and 11(b), and this verifies the validity of our finite-size scaling analysis. We have made the same scaling plot for specific heat at $T=0.265$ and 0.33, and found none of them obeys this scaling formula. This is obviously because at higher temperatures, the phase boundaries of the XY and AF phases start to separate. In fact, those data at higher temperatures are consistent with an Ising transition. As in other figures, a group of nearby data points are calculated from the same simulation with histogram reweighting. The disadvantage of histogram reweighting is that the statistical error in one simulation is replicated by several data points. Therefore, the deviations observed in Fig. 11 as well as Fig. 10 are not real "systematic" deviations, but an artifact of histogram reweighting.

IV. DISCUSSION

Although near the critical magnetic field, the simulation is hindered by the huge correlation length, so that two separate second-order phase boundaries may never be revealed, the staggered magnetization behaves as a rigid spin of nearly fixed length subject to an anisotropic potential. The length of the spin and the form and strength of the anisotropy are predictions of the RG calculation that have been confirmed by our Monte Carlo simulations. Logarithmic corrections of particular forms, which are absent in either first- or second-order phase transitions, have been found in the Monte Carlo simulations in complete agreement with our theoretical predictions. For the phase diagram of the two-dimensional XXZ Heisenberg antiferromagnet with an easy axis, we have thus reached the conclusion that in the thermodynamic limit, the bicritical point appears at $T=0$, with an exponentially narrow paramagnetic phase sandwiched between the low-field AF phase and the high-field XY phase. The location of the bicritical point is "hidden" from detection by "ordinary" means because of finite-size effects that must be carefully analyzed.

In the simulation of any finite-size system, the staggered magnetization remains nonzero on the spin-flop line, which only becomes two separate phase boundaries in the thermodynamic limit. The Ising-like or *XY*-like critical behavior near the spin-flop transition is also expected to be seen in an exponentially narrow range of magnetic field. Our results should be valid for all two-dimensional Heisenberg antiferromagnets or ferromagnets with short-range interaction and easy-axis anisotropy of different forms, since their long-length-scale physics is described by the same Hamiltonian. Due to the finite experimental resolution, including effects from the inhomogeneity in magnetic field and disorder in samples, and possible crossover to three-dimensional behaviors, we expect experiments would only reveal apparent first-order spin-flop transitions and an apparent bicritical point at finite temperature. Also symmetry-breaking perturbations, e.g., crystal fields of square symmetry, are highly relevant to the bicritical phenomena in $2+\epsilon$ dimensions as well as the intricate correlations in the *XY* phase.[3,28] As a result, both the AF phase and the "*XY*" phase might have discrete symmetries, so that the two second-order phase boundaries are likely to be reduced to a first-order phase boundary.

V. CONCLUSION

We have carried out extensive Monte Carlo simulations for a two-dimensional anisotropic Heisenberg antiferromagnet near the spin-flop transition and performed a finite-size scaling analysis based on the anisotropic nonlinear σ model in the regime where the correlation length is much larger than the system size. We have found that, although the finite-size effects tend to obscure the asymptotic behavior, the results of the Monte Carlo simulations are perfectly consistent with the RG calculation for the spin-flop transition and that the bicritical point is at $T=0$.

ACKNOWLEDGMENTS

We thank K. Binder and S. Mitchell for very helpful discussions and suggestions. This research is supported by the Department of Energy through the Laboratory Technology Research Program of OASCR and the Computational Materials Science Network of BES under Contract No. DE-AC05-00OR22725 with UT-Battelle LLC, and also by NSF Grant No. DMR-0341874.

[1] M. Holtschneider, W. Selke, and R. Leidl, Phys. Rev. B **72**, 064443 (2005).
[2] D. P. Landau and K. Binder, Phys. Rev. B **24**, 1391 (1981).
[3] R. A. Pelcovits and D. R. Nelson, Phys. Lett. **57A**, 23 (1976).
[4] D. R. Nelson and R. A. Pelcovits, Phys. Rev. B **16**, 2191 (1977).
[5] J. M. Kosterlitz and M. A. Santos, J. Phys. C **11**, 2835 (1978).
[6] R. A. Cowley, A. Aharony, R. J. Birgeneau, R. A. Pelcovits, G. Shirane, and T. R. Thurston, Z. Phys. B: Condens. Matter **93**, 5 (1993).
[7] J. M. Kosterlitz, D. R. Nelson, and M. E. Fisher, Phys. Rev. B **13**, 412 (1976).
[8] D. P. Landau and K. Binder, Phys. Rev. B **17**, 2328 (1978).
[9] M. E. Mermin and H. Wagner, Phys. Rev. Lett. **17**, 1133 (1966).
[10] A. M. Polyakov, Phys. Lett. **59B**, 79 (1975).
[11] E. Brézin and J. Zinn-Justin, Phys. Rev. Lett. **36**, 691 (1976).
[12] E. Brézin and J. Zinn-Justin, Phys. Rev. B **14**, 3110 (1976b).
[13] A. Aharony, Phys. Rev. B **18**, 3328 (1978).
[14] X. Hu, Phys. Rev. Lett. **87**, 057004 (2001).
[15] Y. Miyatake, M. Yamamoto, J. J. Kim, M. Toyonaga, and O. Nagai, J. Phys. C **19**, 2539 (1986).
[16] D. Loison, C. Qin, K. D. Schotte, and X. F. Jin, Eur. Phys. J. B **41**, 395 (2004).
[17] C. Zhou, M. P. Kennett, X. Wan, M. Berciu, and R. N. Bhatt, Phys. Rev. B **69**, 144419 (2004).
[18] K. Binder and D. P. Landau, Phys. Rev. B **30**, 1477 (1984).
[19] M. E. Fisher, Phys. Rev. Lett. **34**, 1634 (1975).
[20] D. R. Nelson and J. Rudnick, Phys. Rev. Lett. **35**, 178 (1975).
[21] D. R. Nelson, in 0, edited by J. J. Becker, G. H. Lander, and J. J. Rhyne, AIP Conf. Proc. No. 29 (AIP, New York, 1976).
[22] J. Rudnick and D. R. Nelson, Phys. Rev. B **13**, 2208 (1976).
[23] M. E. Fisher and D. R. Nelson, Phys. Rev. Lett. **32**, 1350 (1974).
[24] M. E. Fisher, Rev. Mod. Phys. **46**, 597 (1974).
[25] L. P. Kadanoff, A. Houghton, and M. C. Yalabik, J. Stat. Phys. **14**, 171 (1976).
[26] J. M. Kosterlitz and D. J. Thouless, J. Phys. C **6**, 1181 (1973).
[27] P. Peczak and D. P. Landau, Phys. Rev. B **43**, 1048 (1991).
[28] E. Rastelli, S. Regina, and A. Tassi, Phys. Rev. B **70**, 174447 (2004).